Radiating-Edge Plasma Experiments on JET

G P Maddison 1), M Brix 2), R Budny 3), M Charlet 1), I Coffey 1), G Cordey 1), P Dumortier 4), S K Erents 1), N C Hawkes 1), M von Hellermann 5), D L Hillis 6), J Hogan 6), L D Horton 7), L C Ingesson 5), S Jachmich 2), G L Jackson 8), A Kallenbach 7), H R Koslowski 2), K D Lawson 1), A Loarte 9), G F Matthews 1), G R McKee 8,10), A Meigs 1), A M Messiaen 4), F Milani 1), P Monier-Garbet 11), M Murakami 6,8), M F F Nave 12), J Ongena 4), M E Puiatti 13), E Rachlew 14), J Rapp 2), S Sharapov 1), G M Staebler 8), M Stamp 1), J D Strachan 3), G Telesca 13), M Z Tokar 2), B Unterberg 2), M Valisa 13), K-D Zastrow 1), & EFDA-JET 2000 workprogramme contributors[*]

1) EURATOM/UKAEA Fusion Association, Culham, UK
2) IPP, Forschungszentrum Jülich GmbH, EURATOM Association, D-52425 Jülich, Germany[†]
3) Princeton Plasma Physics Laboratory, Princeton University, NJ 08543, USA
4) LPP / ERM-KMS, Association EURATOM-Belgian State, B-1000 Brussels, Belgium[†]
5) FOM-IVP, EURATOM Association, Postbus 1207, NL-3430 BE Nieuwegein, Netherlands[†]
6) ORNL, Oak Ridge, TN 37831-8072, USA
7) Max-Planck IPP, EURATOM Association, D-85748 Garching, Germany
8) DIII-D National Fusion Facility, San Diego, CA 92186-5698, USA
9) EFDA-CSU, D-85748 Garching, Germany
10) University of Wisconsin-Madison, Madison, Wisconsin, USA
11) CEA Cadarache, F-13108 St Paul lez Durance, France
12) CFN, EURATOM-IST Associação,1096 Lisbon, Portugal
13) Consorzio RFX, Corso Stati Uniti 4, 35127 Padova, Italy
14) Association Euratom-NFR, KTH, Stockholm, Sweden

[*] see Appendix in post-deadline paper of J Pamela [†] Partners in the Trilateral Euregio Cluster (TEC).

e-MAIL address of first author : geoff.maddison@ukaea.org.uk

Abstract. Scaling to larger tokamaks of high confinement plasmas with radiating edges is being studied through internationally collaborative experiments on JET. Three different configurations have been explored. A small number of limiter L-mode discharges have most closely repeated the approach used on TEXTOR-94. Divertor L-modes at intermediate density have pursued transiently improved states found on DIII-D. An original scheme has also examined impurity seeding of higher density ELMy H-modes, formed either in a novel pumped-limiter like arrangement, or again in divertor geometry. While strongly peaked density profiles thought to be important in TEXTOR-94 have not generally been produced, nevertheless beneficial effects have similarly emerged in JET. Confinement up to H-mode quality, together with radiation fractions of ≈ 40%, has briefly been obtained in divertor L-modes. Most notably, ELMy H-mode confinement has been sustained at densities close to the Greenwald level, with little change of central Z_{eff} but up to ≈ 60% radiation, in long, "afterpuff" phases following the end of main gas fuelling. Outstanding products of normalized confinement and normalized density $H_{97} \cdot f_{\mathrm{Gwd}} \approx 0.9$ have consequently been achieved. Marked reductions in the frequency of accompanying ELMs are generally also induced.

1. Introduction

In a burning next-step plasma, it will be necessary simultaneously to achieve sufficient confinement, density, and purity, together with acceptable exhaust of energy and particles, all these properties being sustained for some hundreds of confinement times. One approach is based upon the tokamak steady H-mode, but difficulties remain with intense loads repetitively imposed upon bounding surfaces by the large ELMs which tend to accompany its best conditions [1,2]. A possible recourse has been exemplified on the TEXTOR-94 pumped-

limiter device, where the plasma edge is “seeded” with medium-Z impurities to increase the fraction of power dispersed as mantle radiation. This intervention has further produced a spontaneous transition to a so-called “radiative improved” (RI) state [3], having confinement up to H-mode value, density up to or exceeding Greenwald level [4], plus long stationarity and good edge retention of impurities, in addition to high radiation and no ELMs. It is essential, therefore, next to investigate scaling of this regime, in which all next-step requirements might be realized together, both to larger and to diverted plasmas. Joint experiments have consequently been initiated on JET.

The programme pursued is briefly reviewed in the following sections. A small number of cases so far have addressed limiter L-modes, so most closely approaching the discovery method of TEXTOR-94. First confinement gains from seeding of diverted plasmas have been demonstrated transiently on DIII-D [5], and hence such intermediate density L-modes have also been investigated. Most attention to date though has been devoted to higher density ELMy H-modes, to test adaptation of this favoured next-step regime. Both magnetic equilibria used and seed species injected have been varied. Finally, the present status is summarized and continuing studies are outlined.

2. Limiter plasmas

The closest configuration in JET to that of RI-modes in TEXTOR-94, although with much weaker wall and target surface pumping only, involves moderately elongated ($\kappa \approx 1.4$) plasmas formed against its 12 discrete outboard carbon limiters [6]. Partly to assist power handling on these elements, $B_0 = 2.9$ T, $I_p = 1.8$ MA yielding $q_a \approx 5$ were chosen. Up to 8 MW of NBH were applied, and with no other gas fuelling except from impurity seeding with neon, Greenwald density fraction $f_{Gwd} \equiv \pi \{ \bar{n}_e \; 10^{20} \; m^{-3} \} \{ a^2 \; m^2 \} / \{ I_p \; MA \}$ up to $\approx 80\%$, radiation fraction $f_{rad} \equiv P_{rad} / P_{input}$ up to $\approx 70\%$, for central line-average $Z_{eff} \leq 4$, were reached. However, confinement was only slightly increased relative to L-mode performance measured by the ITERH89P scaling law $H_{89} \equiv \tau_E / \tau_{H89P}$ [7], viz $H_{89} \approx 1.3$, and even this *normalized*

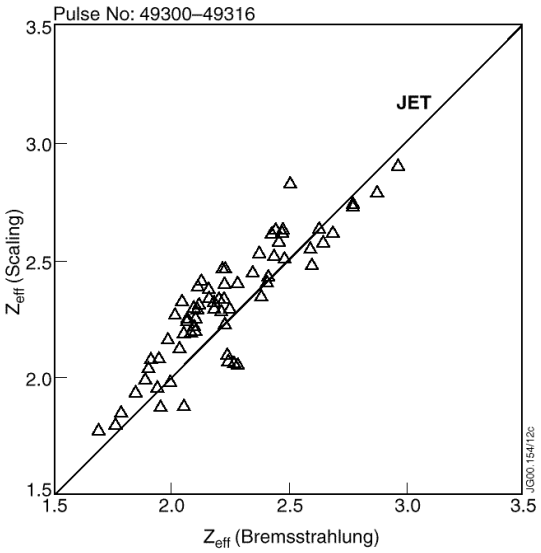

FIG.1 Comparison for JET limiter L-modes with Ne (multiple points per shot) of measured Z_{eff} versus values from Matthews scaling, using tomographic reconstruction of total radiation.

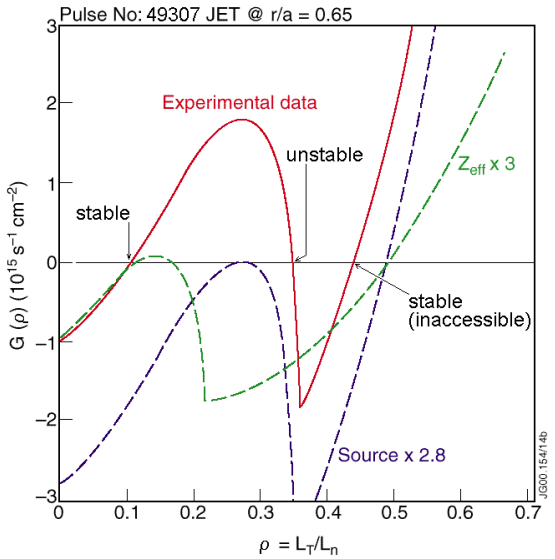

FIG.2 Difference between particle flux and integrated source distribution for JET limiter L-mode with Ne, having roots at G = 0 [9]. The upper RI-like solution remains inaccessible. Threefold increases of Z_{eff} or sources would be needed to admit higher r (see text).

quantity tended to decline with input power. Conditions were limited by appearance both of lower inboard MARFEs, and a lobe of strong emission in the upper inboard region. The latter may not be axisymmetric, but still is probably due to limiter and / or wall tile interactions, consistent with spectroscopic observations that carbon remained the dominant impurity [6]. Allowing for this top inboard light, total radiated power then conforms well with the Matthews scaling [8], as illustrated in Fig.1 by comparing measured with predicted $Z_{\rm eff}$ values. Hence impurity behaviour still resembled that prevailing in other experiments.

A key distinction was that density profiles in JET tended to remain comparatively flat, $n_e(0)/\langle n_e\rangle_{\rm vol} \le 1.6$, as opposed typically to ≈ 2.6 for RI-modes at similar q_a in TEXTOR-94 [3]. Inboard injection of deuterium pellets did not alter JET peaking either. Current understanding of the RI transition would identify this as crucial, since improved confinement is suggested to arise from reduction of ion temperature gradient (ITG) transport upon added impurities leading to attainment of sufficient density peaking [9]. A bifurcation to such conditions may be described by their lowering an integral continuity constraint $\Gamma_r - (1/r)\int_0^r S_e\, r\, {\rm d}r \equiv G(\rho) = 0$, where S_e are particle sources and $\rho \equiv L_T/L_n = 1/\eta_i$ is the ratio of gradient scale-lengths, until its higher ρ root suppressing ITG instabilities becomes accessible [9]. Applying the same analysis to JET conditions finds the latter is denied, as shown in Fig.2, consistent with experimental results [6]. Roughly a threefold increase of either $Z_{\rm eff}$ or interior sources separately would be needed to reach a transition under these circumstances.

3. Divertor L-modes

In the DIII-D tokamak, increases in confinement have been induced by impurity seeding of divertor L-modes, so retaining their less intense, ELM-free edge properties [5]. The gains up to H-mode level are generally transient, preceding onset of neo-classical tearing modes and sawteeth (although then H_{89} remains significantly > 1), but importantly occur at lower density, $f_{\rm Gwd} \approx 40\%$. Similar physics trials have been conducted in JET, using the standard vertical targets configuration of its MkIIGB divertor [1]. Scans of toroidal field strength, input power, and timing of neon injection have primarily been examined to date. A representative discharge scheme at $B_0 = 2.2$ T, $I_{\rm p} = 1.7$ MA with ramped heating and early seeding is

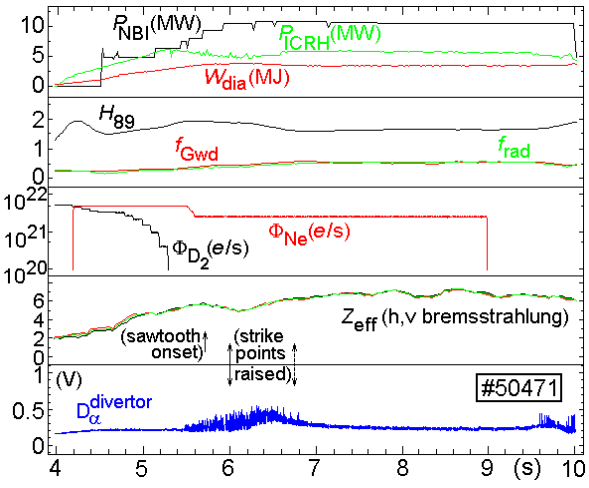

FIG.3 Sample divertor L-mode with Ne seeding in JET, showing: heating & stored energy; confinement, density & radiation factors; gas inputs; $Z_{\rm eff}$; divertor Da .

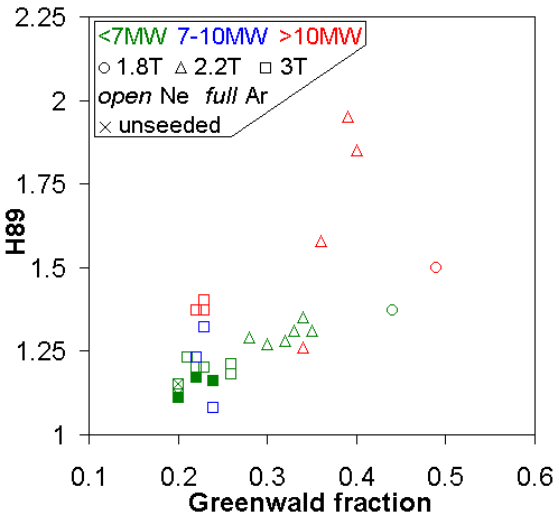

FIG.4 Normalized confinement versus normalized density for JET divertor L-modes (one point per shot): different magnetic field; total input power; seed species.

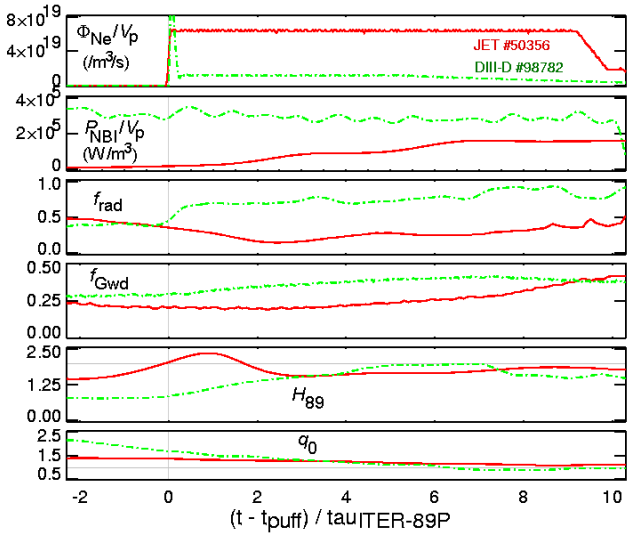

FIG.5 Properties for DIII-D and JET divertor L-modes with Ne seeding in non-dimensional-ized time: Ne input and P_{NBI} over plasma volume; radiation, density and confinement factors; central saftey factor.

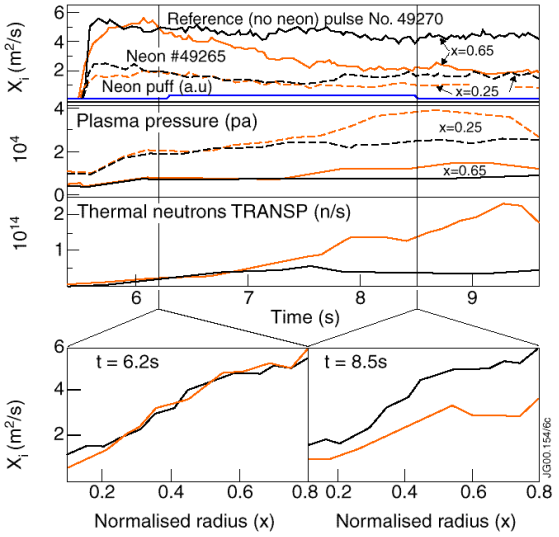

FIG.6 Ion thermal diffusivity and plasma pressure at two normalized radii, plus thermal neutron emission, from the TRANSP code for paired JET 3T divertor L-modes without & with Ne seeding.

illustrated in Fig.3. Although the divertor Dα emission remains low and irregular, normalized confinement in particular rises briefly to $H_{89} \approx 2$ while $f_{\rm rad}$, $f_{\rm Gwd} \approx 40\%$. In this case, the latter occur for lower power and H_{89} declines again before the steady heating phase is reached, but the mechanism involved remains unclear since typically sawteeth also begin around this roll-over point (the strike-points are raised too in the pulse shown, settling at their higher position from the dashed arrow onwards). In addition, ICR heating has been applied to some plasmas, as depicted, though no significant delay of sawteeth has yet been derived, despite Alfven magnetic signatures of fast particle populations appearing.

A survey over cases, mainly involving neon, is presented in Fig.4. There is little indication of any confinement dependence on magnetic field strength, best results in fact emerging at higher Greenwald fractions, and above all for higher input power at moderate field. These latter JET pulses achieve H_{89}, $f_{\rm Gwd}$ parameters and durations quite close to those of DIII-D experiments, as revealed by superimposing respective traces in dimensionless time, normalizing each by its mean $\tau_{\rm H89P}$ value following the start of seeding (Fig.5). A notable feature is that while neon input per unit volume is larger in JET, its rise of radiated power is much slower, this delayed response actually being a general distinction from DIII-D. Similar H_{89} is thus achieved for lower $f_{\rm rad}$ in JET. In contrast to TEXTOR-94 RI-modes too, DIII-D seeded L-modes tend not to exhibit strong density peaking, and for the JET cases shown highest confinement factors indeed occur for lowest values of $n_e(0)/\langle n_e\rangle \approx 1.5$. Analyses with the TRANSP local transport code for a shot pair without and with neon at 3 T indicate a progressive decrease at least of ion thermal diffusivity across the whole plasma, correlated with rising pressure and neutron emission, during neon input (Fig.6) [10]. At the same time, Thomson scattering measurements show no systematic perturbation of electron temperature profiles, so the effect is not merely a gyro-Bohm reduction due to cooling. Calculations also with the GKS gyro-kinetic code in turn do suggest suppression of ITG modes, though countered somewhat by emergence of dissipative trapped electron (DTE) modes [10]. Another candidate for the mechanism of stabilization is strongly sheared rotation, especially with unbalanced NBI as here in JET. Charge-exchange spectroscopic detection of toroidal rotation in the highest H_{89} plasmas at 2.2 T, however, discloses no sharp gradients or temporal

developments of the angular velocity, so within the uncertainties, concentrated shear seems not to be evident at least in this component of the motion.

4. ELMy H-modes

As mentioned above, there is an impetus to try to combine into ELMy H-modes some of the benefits found for radiative mantle plasmas. In JET, a novel arrangement is provided by lowering the magnetic X-point onto or just inside the barrier dividing inboard and outboard sides of its MkIIGB divertor, yielding the so-called "septum" configuration (Fig.7). Reduced divertor pumping through the deepened edge results in a system reminiscent of a pumped limiter. It has been observed that the power threshold for entry into H-mode is lower in septum plasmas than in conventionally diverted discharges [11]. Thus they may have a greater capacity for increased radiated power through seeding without falling back below the H-mode boundary. Initial trials examined neon or argon injection during the main fuelling phase of discharges [12], but as in the so-called density limit [13], gas input itself is known to be able adversely to affect H-mode confinement. Attention has therefore been turned to long phases following main gas puffing, designated "afterpuff" stages. Sets of pulses have been executed, progressing from no gas fuelling to determine the "natural" state, to deuterium fuelling only, then adding neon or argon. Septum tests at normal triangularity ($\delta^u = 0.18$) have been contrasted with ones having higher shaping ($\delta^u = 0.33$) since this can modify ELMs, and also with diverted plasmas placing the strike-points in the bottom corners of the MkIIGB structure in order to maximize pumping and so best expose its influence. Impurities were first injected during the period of main puffing, then smaller inputs were also included afterwards to help sustain more stationary conditions. A very low influx of D_2 did not degrade performance either, and actually helped

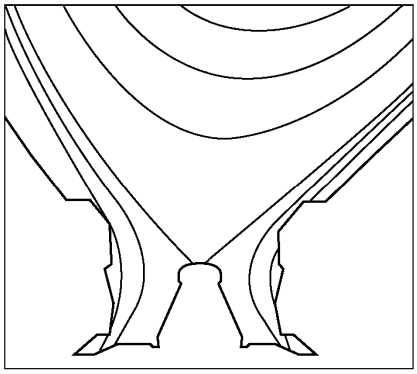

FIG.7 Lower region of JET "septum" configuration.

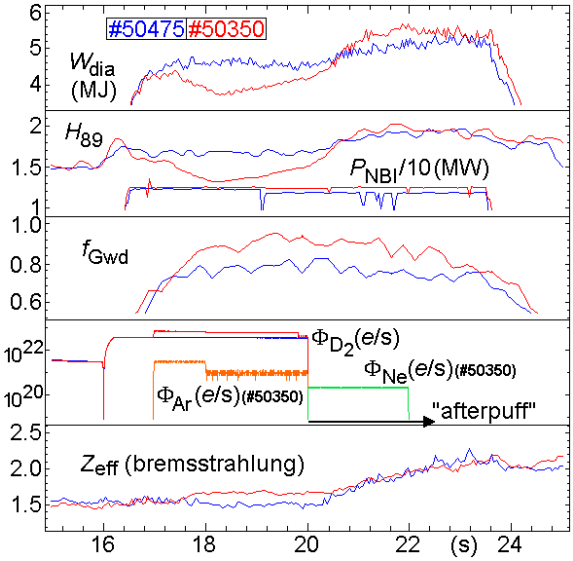

FIG.8 Septum ELMy H-modes in JET without (#50475) and with (#50350) impurity seeding, demonstrating "afterpuff" stages. Traces similar to those in Fig.3.

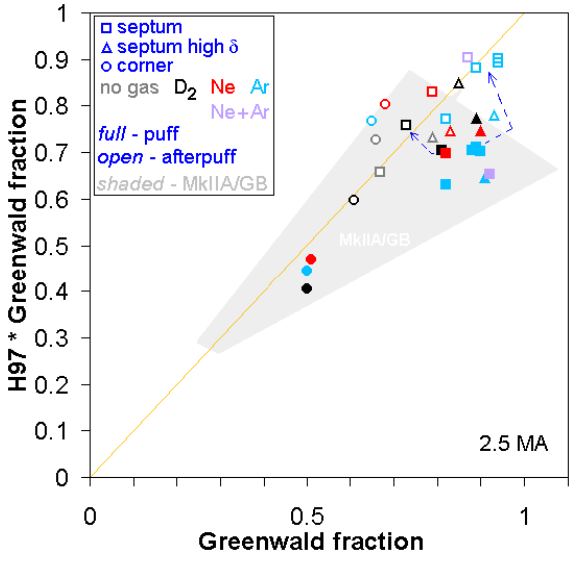

FIG.9 Figure-of-merit for JET ELMy H-modes in septum & corner configurations, puff & afterpuff stages of each shot. Shading indicates general results in MkIIA/GB without seeding.

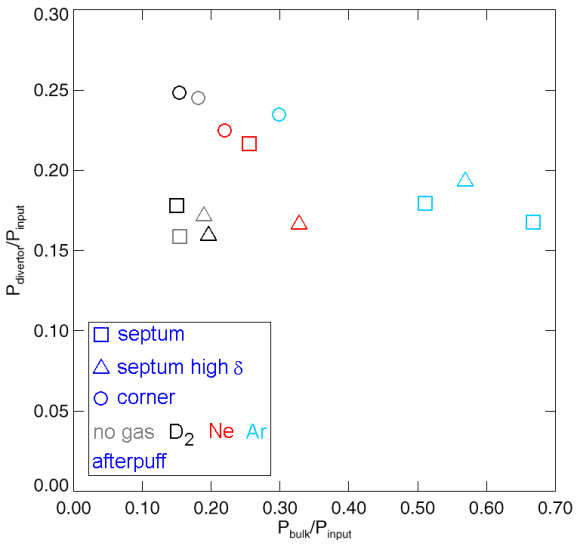

FIG.10 Fraction of power radiated in the divertor & X-point against the main plasma fraction, derived from tomographic reconstruction. Late / afterpuff stages only.

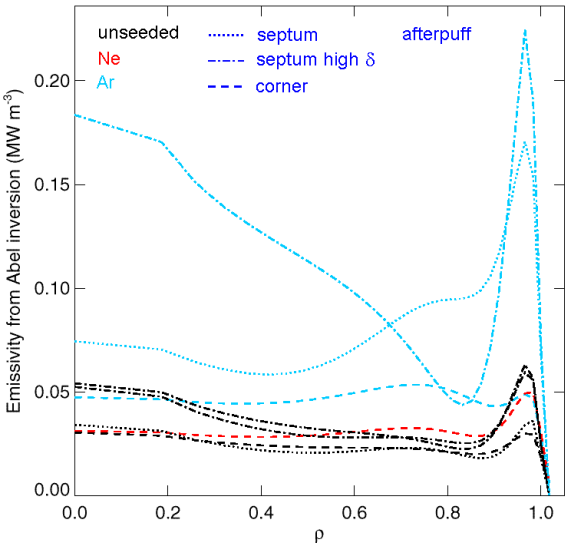

FIG.11 Profiles of radiated power density against normalized radial coordinate, from Abel inversion (no-gas and D_2 only cases not distinguished). Afterpuff stages only.

to lower the carbon content. Representative schemes at $B_0 = 2.4$ T, $I_p = 2.5$ MA without and with impurity seeding are contrasted in Fig.8 (illustrating the single instance so far in which Ar seeding during main puffing was combined with Ne afterwards). It is seen that stored energy and normalized confinement rise in the afterpuff stage in both situations, but when impurities are introduced *higher normalized density is maintained* as well. Maximum properties are sustained for a time $\approx 3\tau_E$, during which preliminary calculations with TRANSP do determine significantly decreased thermal diffusivities for both ions, and the effective coefficient describing total transport, across most of the plasma cross-section. There is little evidence of density peaking, however, with $n_e(0)/\langle n_e \rangle < 1.5$ prevailing in every example. A crucial aspect is that higher radiation fraction is achieved without significant increase of Z_{eff}, values of $f_{rad} \approx 60\%$ being obtained in septum afterpuffs with Ar for approximately no change in Z_{eff} relative to unseeded references.

Results are summarized in Fig.9, using the dimensionless figure-of-merit $H_{97} \cdot f_{Gwd}$ [1], where now confinement is normalized to the ITERH97 scaling law $H_{97} \equiv \tau_E / \tau_{H97}$ [14]. One point is shown in the steady part of puff and afterpuff phases of each gas-fuelled shot. The shaded area indicates accumulated data from unseeded JET MkIIA/GB divertor plasmas at the same current of 2.5 MA. Septum points generally lie towards the top of this range around $f_{Gwd} \approx 70\% - 90\%$ even with just D_2 fuelling (black squares, triangles), and are further improved when impurities are injected (coloured squares, triangles). Their effect upon entering afterpuff stages is portrayed by the dashed arrows. Without seeding, the rise in confinement generally proceeds by moving to lower density, but with radiating impurities H_{97} increases essentially at constant f_{Gwd}. Hence the same good confinement is recovered but at higher density and very high values of their product $H_{97} \cdot f_{Gwd} \approx 0.9$ are achieved. The progressive enhancement is best demonstrated by the sequence of septum afterpuffs from no gas through to Ar and combined Ar + Ne (open squares). Inspection of Dα photon fluxes from the divertor and main torus reveals no obvious changes in recycling sources, but radiating impurities thus appear to be moderating the decline in fuelling efficiency underlying the usual H-mode density limit [13] (eg as in the far corner of the shaded area at $f_{Gwd} > 1$).

Integrating over tomographic reconstructions from bolometry, the fractions of power radiated in the divertor and main plasma above the X-point during afterpuffs are plotted in Fig.10. Unsurprisingly the "corner" diverted configuration has more radiation at and below the X-point, while this fraction changes little with impurities. As required to form a radiating mantle, though, a substantial increase of that from the main plasma accompanies particularly Ar seeding. This conforms with more total radiation being produced for a given Z_{eff} from Ar than Ne, as had been noted before [12]. Much of the enhanced bulk emission is indeed concentrated within the plasma periphery, according to Abel inverted profiles of power density shown in Fig.11. However, central peaking of the radiation is also sometimes apparent, and a spectroscopic estimate of Ar central abundance assuming coronal equilibrium in one septum case does suggest its slow accumulation. Consistently with Fig.10, an equivalent estimate for the corner afterpuff with Ar remains roughly three times lower.

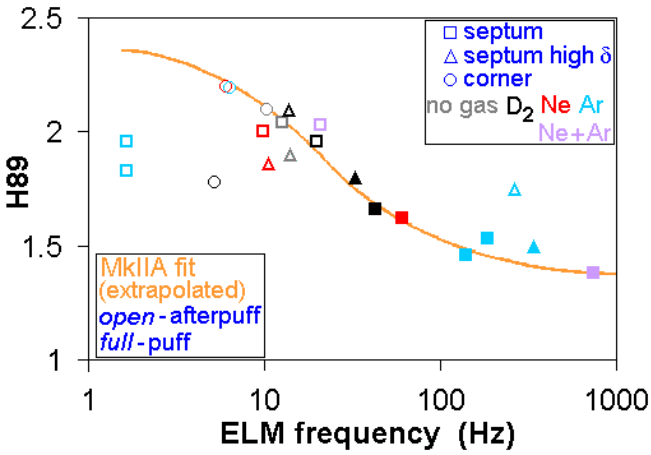

FIG.12 Normalized confinement versus ELM frequency. The line represents the Fishpool fit to MkIIA data, from [2].

During the main puffing, impurity injection tends to enforce Type III ELMs, while there are different effects lasting into the afterpuff. In particular Ar seeding can lead to ELM-free intervals, during which confinement rolls over, and often ending in large ELMs. Neglecting typically small corrections here for fast particles, the electron energy pedestal W_e^{ped} may be approximated from the point of gradient change in edge ECE measurements combined with an interferometer channel at a radius of 3.75 m. Confirmation has then been made against independent assessments from edge Thomson scattering, subject to its slower sampling. No change in W_e^{ped} is apparent for septum afterpuff plasmas, despite a clear rise of total stored energy with H_{89}. Nevertheless, ELM frequencies are considerably reduced with seeding, as

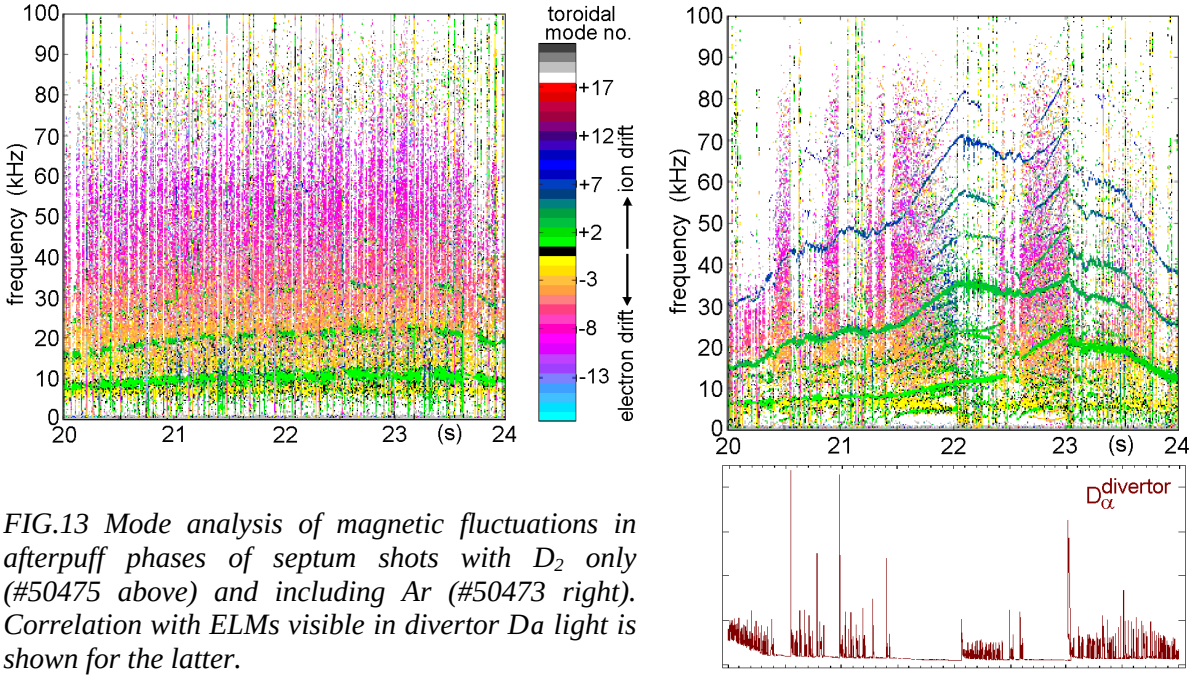

FIG.13 Mode analysis of magnetic fluctuations in afterpuff phases of septum shots with D_2 only (#50475 above) and including Ar (#50473 right). Correlation with ELMs visible in divertor Da light is shown for the latter.

depicted in Fig.12. Those instances exhibiting a strong compound signature and thus uncertain frequency have been excluded. Otherwise ELMs tend to slow considerably from puff to afterpuff stages of septum discharges, especially with Ar as mentioned, and except at very low frequencies still in agreement with the representative scaling deduced for MkIIA experiments [2]. Further studies will examine ELM fractional energy losses $\Delta W / W$ as well, to check how far their magnitudes might be moderated by heightened radiation. A further connotation of ELM alterations, however, is included in Fig.13. Cross-correlated phase differences between fast magnetic signals at two toroidal locations are analysed for their mode structure. Positive numbers correspond to modes rotating in the ion drift direction, negative ones in the electron drift direction. The most striking feature for the septum unseeded afterpuff plasma in Fig.13 is its broad band electron-drift magnetic activity, which in fact is concentrated between its large ELMs (white lines through the spectrum). An equivalent ion-drift effect is not evident. The strong modification of ELMs following Ar injection can be seen markedly to lessen electron-drift modes, and in particular they are suppressed by intervals of small, fast ELMs (eg just after 22 s or 23 s). Interestingly, electron-drift features also gradually decline throughout the long ELM-free interval after ≈ 21.4 s when confinement peaks. These modes are difficult to locate radially, and to relate quantitatively to transport, but indicate the susceptibility of intrinsic plasma fluctuations to radiative impurity seeding.

5. Summary

While radiative states induced by medium-*Z* impurities in JET have not so far reproduced the definitive improvements established in TEXTOR-94, positive benefits still have been found. In divertor L-modes with Ne seeding, confinement factors up to $H_{89} \approx 2$ for radiation and Greenwald fractions $f_{\mathrm{rad}}, f_{\mathrm{Gwd}} \approx 40\%$ have briefly been obtained, closely resembling results in DIII-D. More effective stabilization of sawteeth may allow extension of these regimes. Most notably, in ELMy H-modes limited on the MkIIGB divertor septum, long “afterpuff” phases subsequent to main gas fuelling have attained high confinement *at densities close to Greenwald level* upon introduction of Ne or Ar. Outstanding products $H_{97} \cdot f_{\mathrm{Gwd}} \approx 0.9$ have been achieved. Furthermore radiation fractions have approached $f_{\mathrm{rad}} \approx 60\%$ for almost no deterioration in Z_{eff}, while ELMs are generally lowered in frequency. Maximum properties have been sustained for $\approx 3\tau_E$, during which radiation sometimes tends to peak on axis. Even longer stationarity could therefore be sought in further experiments to test edge retention. Similarly, higher density peaking thought to underlie TEXTOR-94 behaviour could be pursued, perhaps using deep pellet fuelling. These results contribute to the evidence that impurity seeding can benefit integrated plasma performance vital to next-step operation.

Participation of UKAEA authors was supported jointly by the UK Dept of Trade & Industry and Euratom.

References

[1] L D Horton et al Nuc Fus **39** (1999) 1
[2] G M Fishpool Nuc Fus **38** (1998) 1373
[3] J Ongena et al Plas Phys Cont Fus **41** (1999) A379
[4] B Unterberg et al *these proceedings*
[5] G R McKee et al Phys Plas **7** (2000) 1870
[6] B Unterberg et al *to appear in* Proceedings 27th EPS Conference CFPP, Budapest, June 2000
[7] P N Yushmanov et al Nuc Fus **30** (1990) 1999
[8] G F Matthews et al Nuc Fus **39** (1999) 19
[9] M Tokar et al Phys Rev Lett **84** (2000) 895
[10] G L Jackson et al *to appear in* Proceedings 27th EPS Conference CFPP, Budapest, June 2000
[11] L D Horton et al paper P1.021/A (p.193), Proceedings 26th EPS Conference CFPP, Maastricht, June 1999
[12] J D Strachan et al Plas Phys Cont Fus **42** (2000) A81
[13] G Saibene et al Nuc Fus **39** (1999) 1133
[14] J G Cordey et al Plas Phys Cont Fus **39** (1997) B115